ELSEVIER

Fluid mixing and mass transfer in two-dimensional cavities with time-periodic lid velocity

Tatsuo Nishimura and Koji Kunitsugu
Department of Mechanical Engineering, Yamaguchi University, Ube, Japan

Fluid mixing and mass transfer in cavities with time-periodic lid velocity were examined numerically. Unsteady Galerkin finite elements computations were performed for various flow parameters. Global fluid mixing is greatly promoted when an unsteady component of the velocity is superimposed on the steady flow. There is an optimum oscillation frequency that produces the best mixing. Fluid mixing also depends on the oscillation amplitude and the geometric aspect ratio. However, the oscillation frequency has little effect on mass transfer between the walls at different concentrations. It is revealed that excellent global fluid mixing does not always lead to heat and mass transfer enhancement. © 1997 by Elsevier Science Inc.

Keywords: chaotic mixing; mass transfer; oscillatory cavity flow; finite element method

Introduction

Because of the pioneering studies of Aref (1984), Ottino et al. (1992) and others, mixing by chaotic pathlines has become quite familiar to the polymer processing and biomedical applications. This phenomenon has been called chaotic mixing, chaotic advection, or Lagrangian turbulence. In short, it refers to the random path of a fluid particle convected by time-periodic flow with a regular velocity field. This suggests a very intriguing and exciting application—fluid mixing can be achieved with regular laminar flow.

In recent years, several heat and mass transfer investigators have reported that chaotic mixing can greatly enhance heat and mass transfer in several devices (Chang and Sen 1995; Nishimura 1994). Ghosh et al. (1992) numerically studied the enhancement of cross-stream heat transfer by forced oscillations of Stokes flow in an eccentric annulus mixer and found the existence of an optimum frequency for maximum transport enhancement. Similarly, Saatdjian et al. (1995) examined chaotic mixing and heat transfer in the annular region between confocal ellipses. Patera and Mikic (1986) found that small fluid oscillations at the harmonic frequency of the instability dramatically increase the amplitude of the instability, thus heat transfer is enhanced, within a grooved channel, even for Reynolds numbers below the critical value at the onset of self-sustained oscillations. Mackley et al. (1990) studied the effect of fluid oscillation within a baffled tube and showed that excellent heat transfer can be achieved. Nishimura et al. (1993) and Nishimura (1995) studied oscillatory flow and mass transfer in two sinusoidal wavy-walled channels over a wide range of flow parameters, and indicated that inertia-dominated flows yield much better mass transfer enhancement than viscosity-dominated flows. Nishimura and Kojima (1995) also examined the effect of net flow superimposed on oscillatory flow and showed that, at small net flows and large fluid oscillations, the mass transfer rate for pulsatile flow is almost equal to that for oscillatory flow with no net flow.

There is a significant practical advantage in using chaotic mixing to enhance transport rates. Because chaotic mixing can be achieved under laminar flow conditions, the enhanced transport is not associated with enhanced momentum transfer. This is in contrast to transport enhancement by turbulent flow, which usually has significant pressure drop and power expenditure. However, transport enhancement has not been clearly connected with chaotic mixing.

The present study numerically examined the connection between fluid mixing and mass transfer in a simple flow field, as an initial step in a more realistic flow field. The analysis deals with the flow in cavities with time-periodic lid velocity. In this system, time-periodic oscillations lead to chaotic mixing, as reported by Takasaki et al. (1993). They found that there is an optimal frequency producing the best mixing in a square cavity, but did not consider the transport of such diffusing scalars as temperature and concentration of species in this flow field.

Mathematical model and numerical analysis

We consider the unsteady two-dimensional (2-D) laminar motion of an incompressible fluid induced within a cavity with aspect ratio $A = H/L$ by an oscillating top wall, as shown in Figure 1. The top wall velocity is given as follows:

$$v_i(t) = v_s(1 + P \sin 2\pi t/T) \quad (1)$$

where t is the time, v_s the steady component of the velocity, P the amplitude of the oscillating wall velocity, and T the period of oscillation.

Address reprint requests to Prof. T. Nishimura, Department of Mechanical Engineering, Yamaguchi University, Ube-city, Yamaguchi-prefecture 755, Japan.

Received 7 March 1996; accepted 7 January 1997

Int. J. Heat and Fluid Flow 18: 497–506, 1997

655 Avenue of the Americas, New York, NY 10010

0142-727X/97/$17.00
PII S0142-727X(97)00023-4

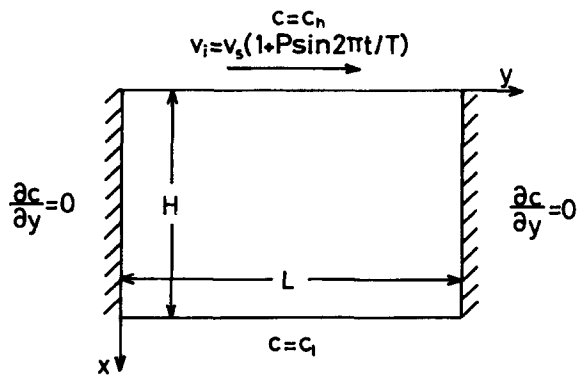

Figure 1 Physical model for fluid mixing and mass transfer

For mass transfer, the oscillating top wall and the bottom wall of the cavity are maintained at uniform concentrations, respectively, c_h and c_l with $c_h > c_l$; zero-flux conditions are supposed on the vertical walls. Buoyancy forces are neglected here.

The governing equations for this problem are given, in nondimensional form, as follows:

Vorticity transport equation:

$$\mathrm{St}\frac{\partial \Omega}{\partial \theta} + V\cdot\nabla\Omega = \frac{1}{\mathrm{Re}}\nabla^2\Omega \tag{2}$$

Relation between vorticity and stream function:

$$\nabla^2\Psi = -\Omega \tag{3}$$

Mass transport equation:

$$\mathrm{St}\frac{\partial C}{\partial \theta} + V\cdot\nabla C = \frac{1}{\mathrm{Pe}}\nabla^2 C \tag{4}$$

where the parameters St, Re, and Pe are, respectively, the Strouhal, Reynolds, and Peclet numbers: $\mathrm{St} = 2\pi L/(v_s T)$, $\mathrm{Re} = v_s L/\nu$, and $\mathrm{Pe} = v_s L/D$.

Equations 2, 3, and 4 are to be solved with no-slip boundary conditions at the walls $U = V = 0$ together with $V = (1 + P\sin\theta)$ at the oscillating top wall and $\Psi = 0$ along the limit of the cavity. Boundary conditions for concentration are $C(A,Y) = 0$ along the bottom wall, $C(0,Y) = 1$ along the oscillating top wall, and $dC/dY(X,0) = dC/dY(X,1) = 0$ along both vertical walls.

Takasaki et al. (1993) examined the effects of the Reynolds number and the frequency of the oscillating top wall on fluid mixing in a square cavity, and they concluded that enhancement of fluid mixing by the imposed oscillation strongly depends on the frequency, but the Reynolds number effect is minute in the range of 50 to 500. The present study also considered the effects of the amplitude of oscillation and geometric aspect ratio, in addition to the frequency effect. The simulations were carried out under the following conditions. The Reynolds and Peclet numbers are fixed at $\mathrm{Re} = 50$ and $\mathrm{Pe} = 50$, respectively; the amplitude of the oscillating wall velocity $P = 0.5$ and 1.5; the Strouhal number $0 < \mathrm{St} < 13$; and the geometric aspect ratio $A = 1/3$, $2/3$, and 1.

Computations were performed using the Galerkin finite element method, which is familiar in numerical analysis (Nishimura et al. 1987, 1992). The characteristics of the algorithm used here are summarized as follows. First, linear triangular elements are used for spatial discretization. Second, the Galerkin method is employed for discretization of the time derivative terms. Third, convective terms are treated explicitly in time, while other terms remain implicit.

Preliminarily, accuracy tests were performed for three cases: steady flow and mass transfer for a square cavity; pulsatile flow in straight-walled channels; and oscillatory flow for a square cavity. In the first case, three nonuniform meshes were defined: 21×21, 31×31, and 41×41 nodal points. The nonuniform mesh provided a higher concentration of nodes near the top and bottom walls of the cavity, where the velocity and concentration gradients need to be accurately resolved. The accuracy tests were conducted in terms of the stream-function value at the central point in the cavity for the several Reynolds numbers less than 400. The criterion for convergence to a steady state satisfied a 10^{-5} maximum relative error for stream function and vorticity. The agreement between 31×31 and 41×41 nodal points was satisfactory, within 1% discrepancies. Also a comparison was performed between the present solutions and the benchmark solutions of Ghia et al. (1982). For example, Figure 2 shows the representative result for the velocity field at $\mathrm{Re} = 400$. The present solution (31×31 nonuniform nodal points) agrees well with Ghia's solution (129×129 uniform nodal points), indicating the effectiveness of nonuniform meshes. For mass transfer, the results of accuracy tests were similar, as well as fluid flow. Figure 3 shows a comparison of mean Sherwood numbers (31×31

Notation

A	geometric aspect ratio, $= H/L$
c	concentration
c_l	concentration at the bottom wall
c_h	concentration at the top wall
C	dimensionless concentration, $= (c - c_l)/(c_h - c_l)$
D	diffusivity
H	height of the cavity
L	length of the cavity
P	amplitude of the oscillating top wall
Pe	Peclet number, $= v_s L/D$
Re	Reynolds number, $= v_s L/\nu$
$S(t)$	summation of an infinitesimal distance between adjacent two particles at time t
Sh	Sherwood number defined by Equation 7
St	Strouhal number, $= 2\pi L/(v_s T)$
t	time
T	period of the oscillating top wall
U	dimensionless vertical velocity
V	dimensionless horizontal velocity
v_i	instantaneous velocity of the oscillating top wall
v_s	steady component of the oscillating top wall
X	dimensionless vertical coordinate
Y	dimensionless horizontal coordinate

Greek

θ	dimensionless time, $= 2\pi t/T$
λ	line stretching
ν	kinematic viscosity
τ	dimensionless time, $= tv_s/L$
Ψ	dimensionless stream function
$\lvert\Psi\rvert_{\max}$	vortex strength
Ω	dimensionless vorticity

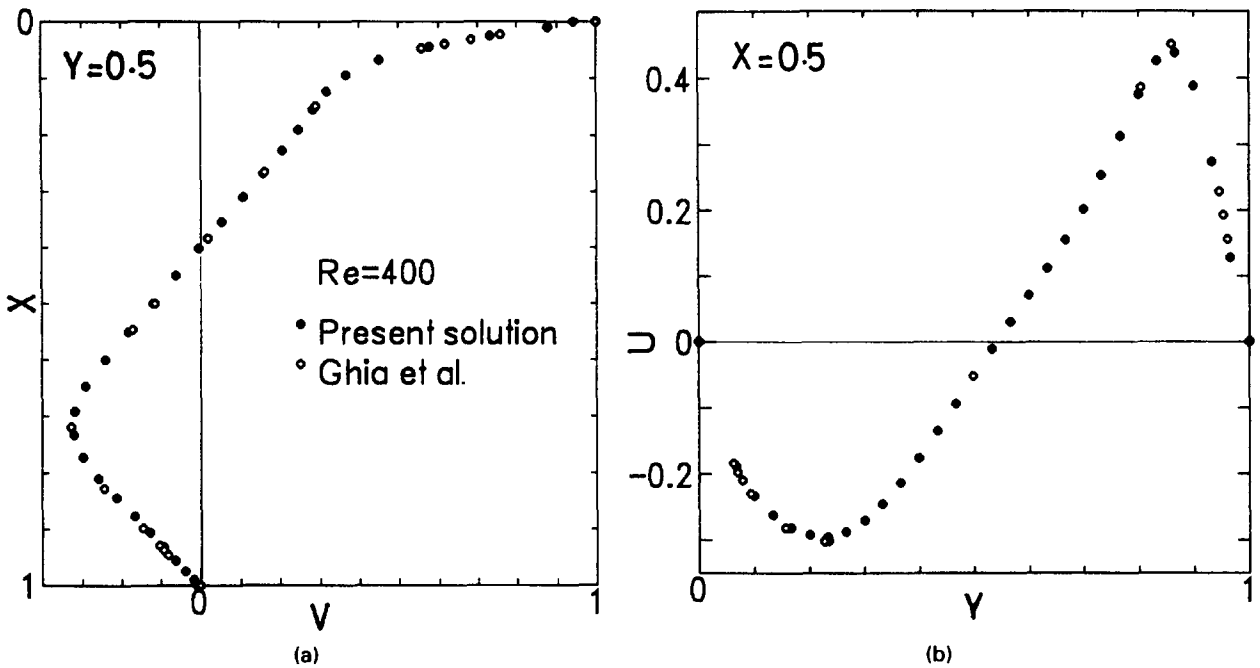

Figure 2 Comparison of the present and other results for a steady cavity flow

nonuniform nodal points) with the solutions (41 × 41 uniform nodal points) by Antonini et al. (1981). The Sherwood number is taken to be the ratio of mass flux attributable to convection and diffusion to that attributable to diffusion alone in the square cavity. The present results lie on the correlation of Antonini et al., in a wide range of Peclet number, which indicates the validity of the numerical analysis for mass transfer.

In the second case, a nonuniform 31 × 31 nodal point was used to compute pulsatile flow in the straight-walled channel, and the numerical time-dependent velocities were compared with analytic ones (Latinopoulos and Ganoulis 1979). The numerical predictions agree well with analytic solutions, even at high frequencies, within 0.5% discrepancies. Furthermore, purely oscillatory flows were compared with the results for several flow parameters by Biringen and Dunabasoglu (1989). A mesh refinement was conducted by using the same ones as the 31 × 31 and 41 × 41 nodal points for steady flow, and there was a satisfactory agreement in the strength of the main vortex, within 1%, and the present solutions also agreed well with those of Biringen and Danabasoglu.

Thus, a typical calculation of time-periodic cavity flows was carried out on 31 × 31 nonuniform nodal points. Because low-Reynolds number flows are focused in this study. However,

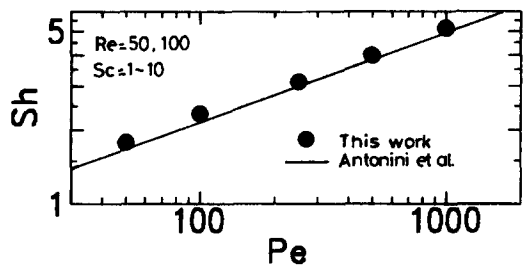

Figure 3 Comparison of the present and other Sherwood numbers for steady flow

additional tests were performed for some flow parameters, and it was confirmed that the present solutions are identical to those with 41 × 41 nodal points. The time-step is chosen to give numerical stability for the convective terms in the vorticity and mass transport equations and typically for these simulations was 0.001. It should be noted that the present numerical solutions are in time-periodic state in which the influence of initial conditions for numerical computations has disappeared.

It is necessary to observe the Lagrangian behavior of the flow field in order to know the fluid mixing as indicated by Ottino et al. (1992). If the fluid velocities are (U,V), then the trajectories of fluid particles are given by

$$\mathrm{St}\, dX/d\theta = U(X,Y,\theta) \tag{5a}$$

$$\mathrm{St}\, dY/d\theta = V(X,Y,\theta) = V(X,Y,\theta) \tag{5b}$$

We assume that at the beginning of calculation a region in the cavity is filled with marked fluid particles. The fluid velocities had been calculated in advance and stored at each time-step throughout the cycle. The particle paths were then determined by interpolation with the nodal point of known velocities to obtain the velocity at the particles' current position. Then a fourth-order Runge–Kutta scheme was used to calculate the particle position after a short time using the known velocity. Once all the particles had been moved, the process could be repeated at the new time. It should be noted that there is no diffusion of particles, and the particles have no substance other than as markers of points within the fluid.

Results and discussion

Fluid mixing

Figure 4 shows instantaneous streamlines during one oscillation cycle for a time-periodic flow in a square cavity (Re = 50, P = 0.5, and St = 4.2). Because the velocity direction at the moving top wall does not change through oscillation, there is only a large clockwise rotating recirculation, indicating a periodic growth and decay in the strength. Figure 5 provides information about mix-

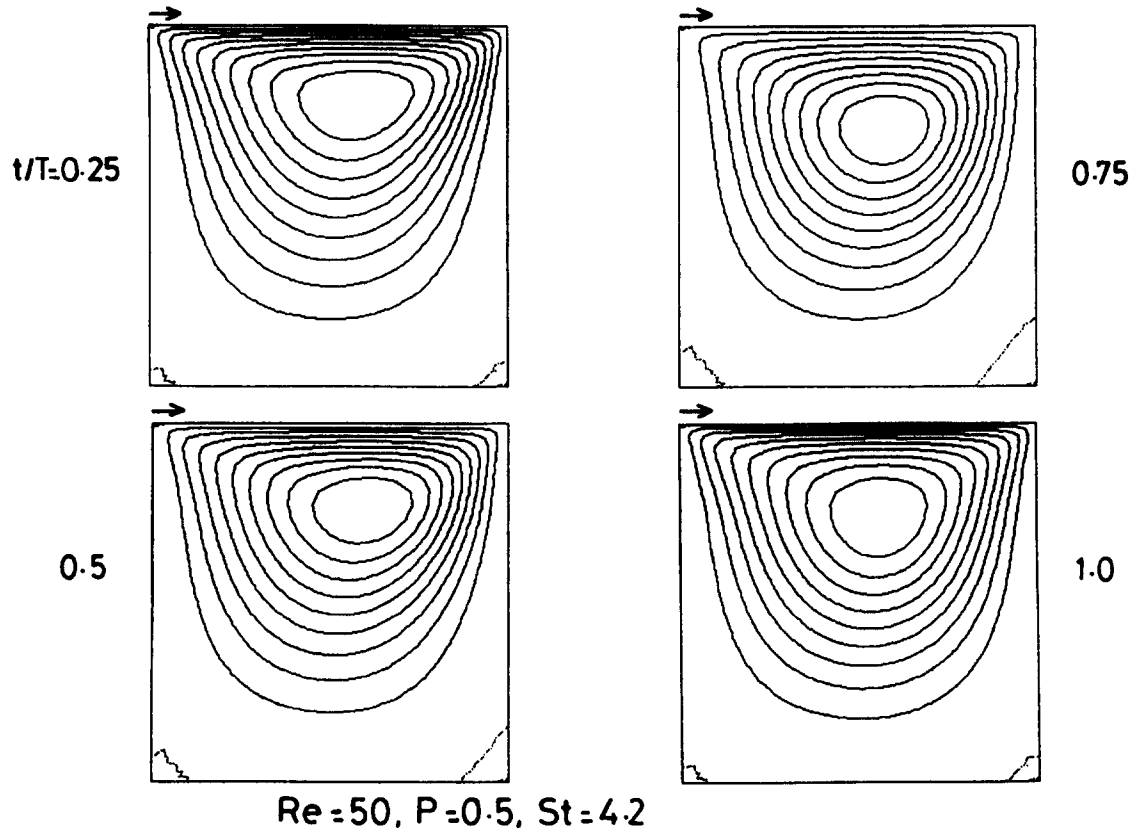

Figure 4 Streamlines for a time-periodic flow (Re=50, P=0.5, and St=4.2)

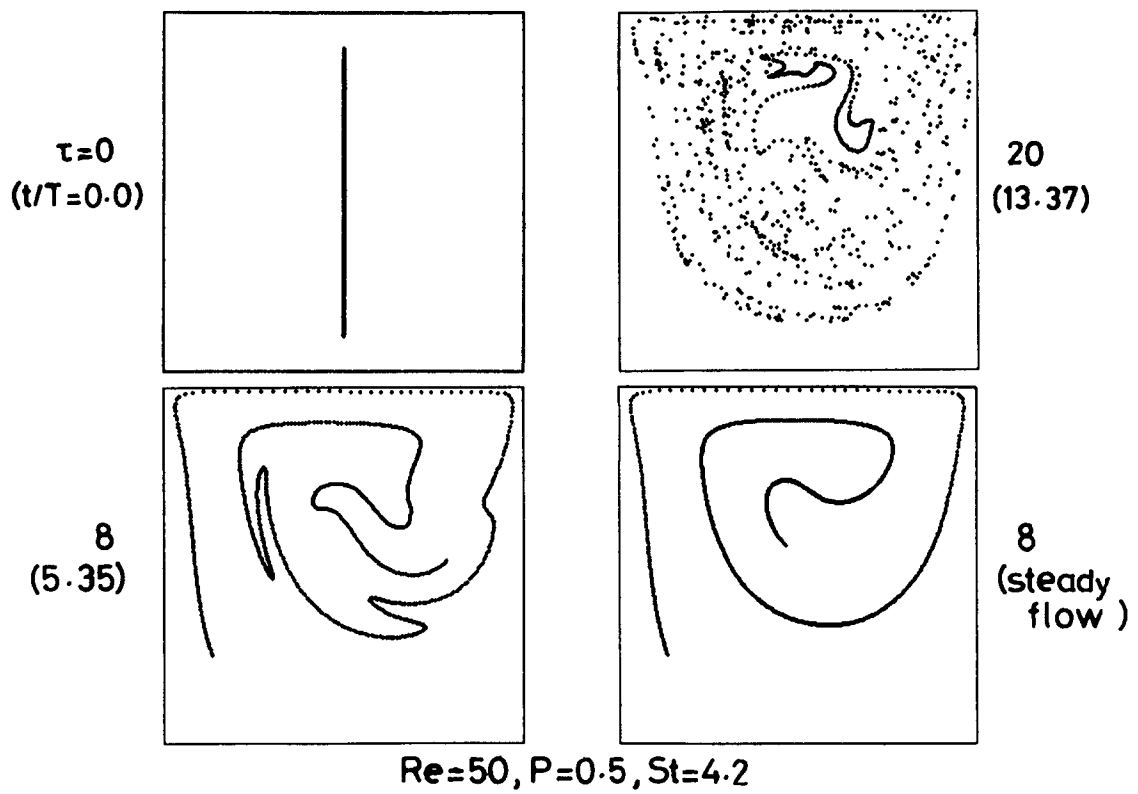

Figure 5 Time evolution of a line of particles (Re=50, P=0.5, and St=4.2)

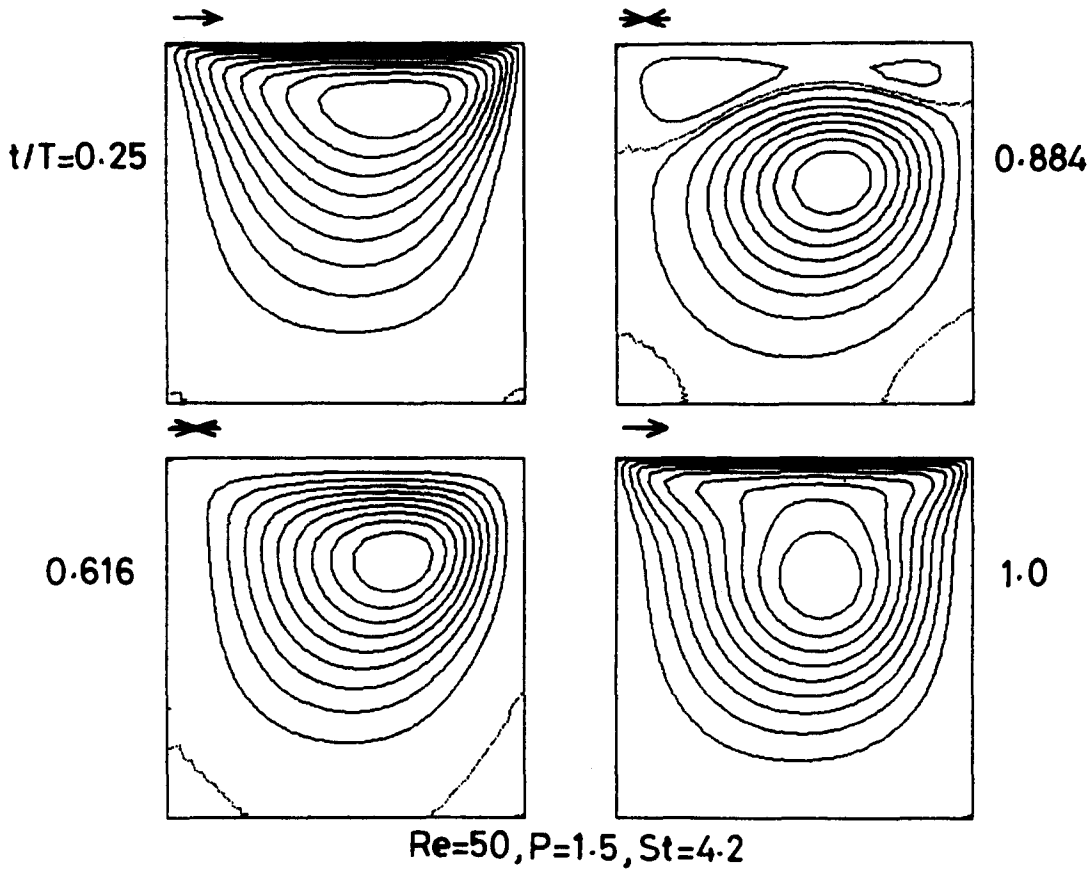

Figure 6 Streamlines for a time-periodic flow (Re=50, P=1,5, and St=4.2)

ing for this time-periodic flow. For reference, the steady flow result is also shown. Initially 1000 particles are placed on the central vertical line in the cavity ($X = 0.1 - 0.9$). Dimensionless time τ is expressed as tv_s/L, which is related to $2\pi t/(\mathrm{St}\,T)$. The line of particles is no longer constrained to follow streamlines. It is striking that much more effective and uniform dispersion of the particles is observed, unlike the steady flow case. In particular, the deformation of the line of particles exhibits the presence of several projections, which are never observed in steady flow. The projections probably enhance fluid mixing; i.e., the stretching and folding process of fluid particles.

When the amplitude of the top wall velocity exceeds unity, the flow direction is reversed. Figure 6 shows streamlines for $P = 1.5$. The clockwise rotating recirculation persists even if the top wall velocity is reversed, and then a counterclockwise rotating recirculation is generated just below the top wall. The center of the clockwise rotating recirculation is found to oscillate along the vertical direction of the cavity, unlike the result for $P = 0.5$ of Figure 4.

Next we consider the effect of Strouhal number corresponding to dimensionless frequency for $P = 1.5$. Figure 7 shows the time variation of the strength of two recirculations; i.e., the clockwise and counterclockwise rotating vortices. A measure of each vortex strength is given by the maximum value of the stream function of the vortex. Although the clockwise rotating vortex is stronger than the counterclockwise vortex, they decrease with increasing Strouhal number. This is because, as suggested from the vorticity transport Equation 2, viscous effects become more dominant than inertial effects as the Strouhal number increases.

Figure 8 shows particle advection at $\tau = 20$ for different Strouhal numbers as an example. The initial position of particles for each flow condition is the same as that shown in Figure 5, and the number of oscillation cycle at $\tau = 20$ depends on Strouhal number. The efficiency of mixing strongly depends on the Strouhal number, and an optimum value of Strouhal number to achieve the best mixing seems to exist. It also seems that at St = 12.57, a poorly mixed region exists near the center portion of the cavity. A square blob of particles is located to clarify the nature of particle advection in this region. Figure 9 shows the results. It is interesting that the particles hardly disperse even after a long

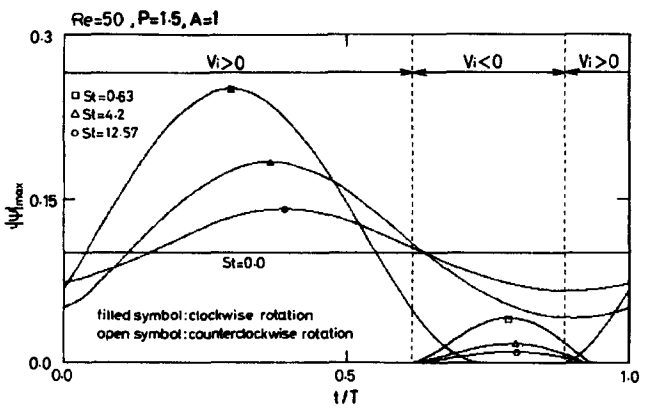

Figure 7 Time variation of vortex strength for different Strouhal numbers (Re=50, P=1.5)

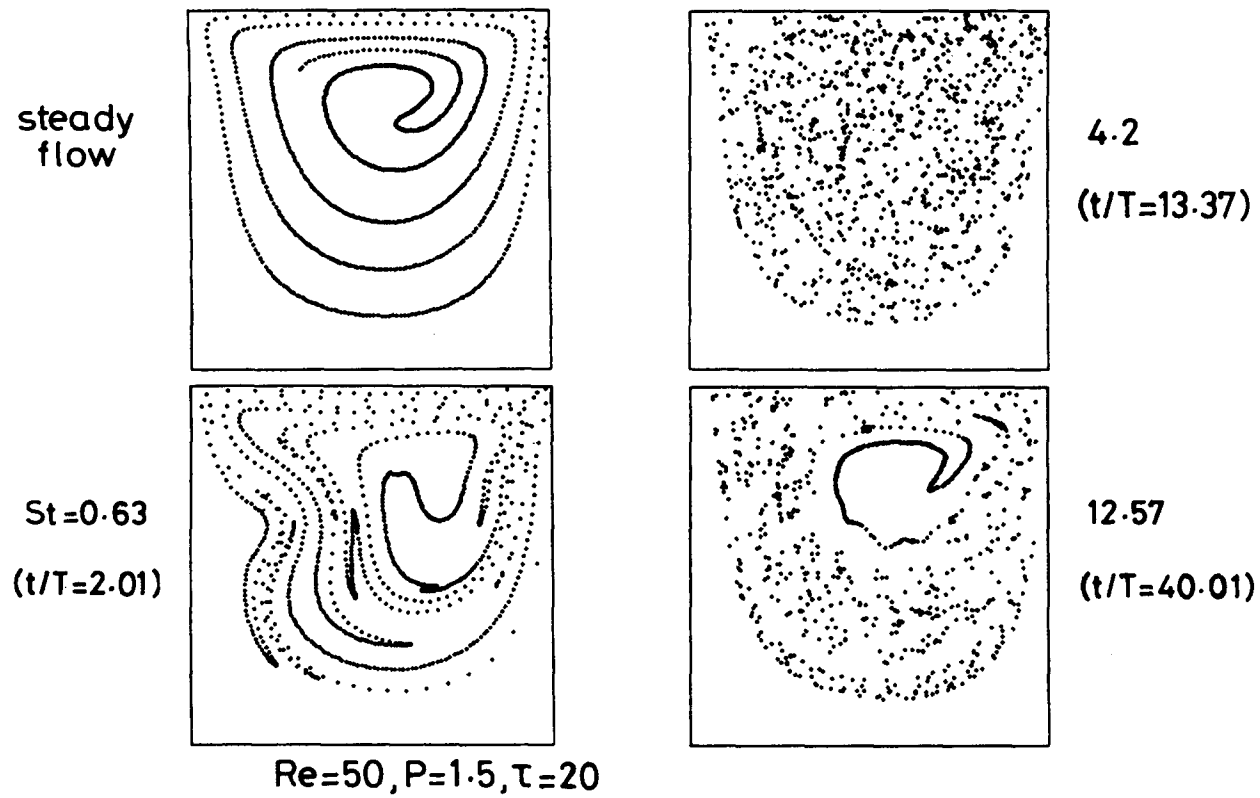

Figure 8 Deformation of a line of particles for different Strouhal numbers (Re=50, $P=1,5$, and $\tau=20$)

time for St = 0.63 and 12.57; i.e., coexistence of well-mixed and poorly mixed regions. Thus the effect of Strouhal number on fluid mixing is not expected from such Eulerian perspectives as the streamline patterns and the time variation of the vortex strength.

Figure 10 shows the effect of the geometric aspect ratio. The fluid mixing is almost identical for $A = 2/3$ and 1, but it is poor for $A = 1/3$. This is because of reduction of the folding process of fluid particles, because the horizontal velocity is more significant than the vertical velocity in the cavity of a small aspect ratio.

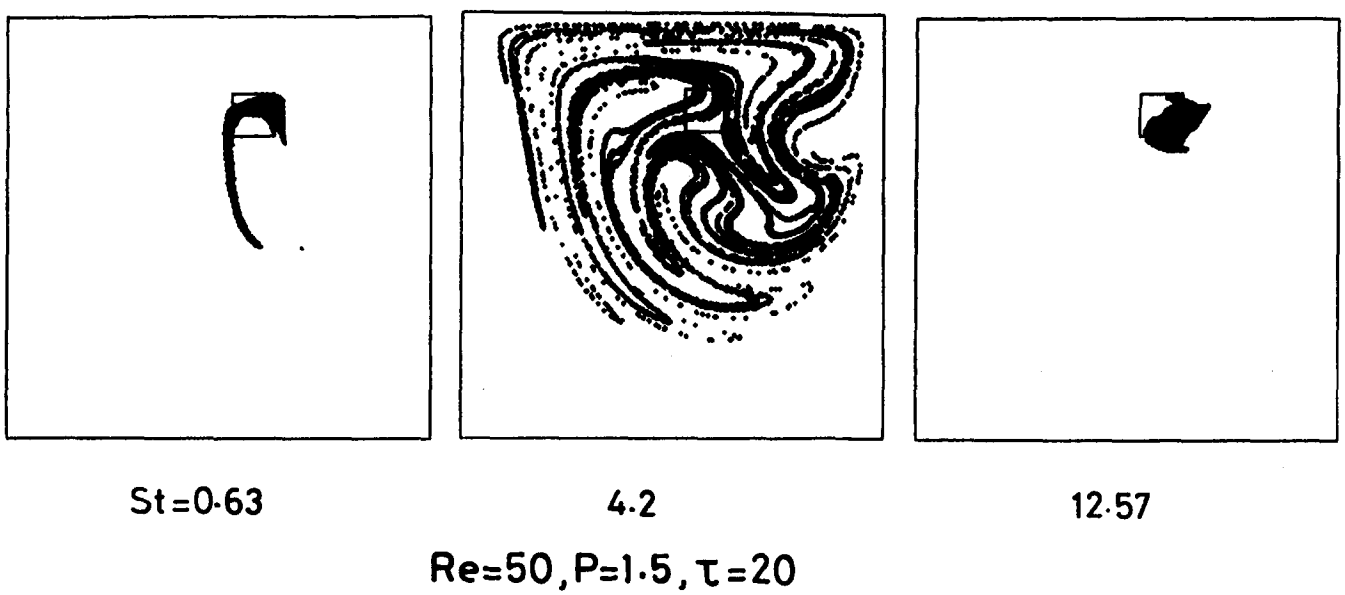

Figure 9 Deformation of a blob of particles for different Strouhal numbers

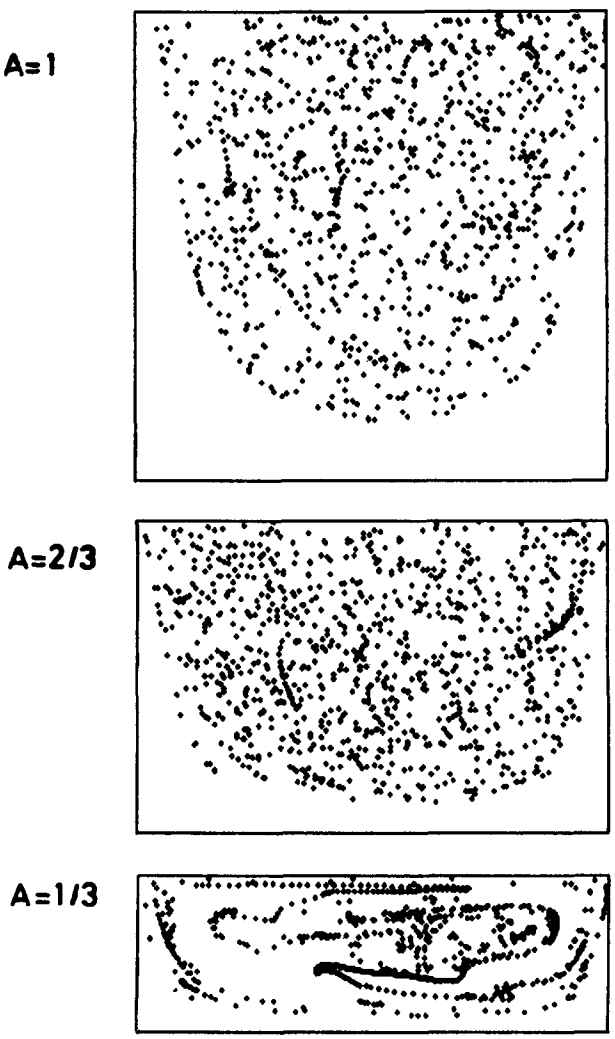

Figure 10 Deformation of a line of particles for different geometric aspect ratios

To quantify the degree of mixing, we consider the stretching of a line of particles. If $S(0)$ is summation of an infinitesimal distance between adjacent two particles on a line of particles for the initial condition as shown in Figure 5, and $S(t)$ is the corresponding change at dimensionless time τ, the line stretching is

$$\lambda = \ln S(\tau)/S(0) \tag{6}$$

Figure 11 shows the time evolution of a line stretching for Re = 50, St = 4.2, $P = 0.5$, and $A = 1$. The line stretching exhibits a great linear growth in terms of exponent during $\tau = 0 - 20$. However, after $\tau = 20$, it tends to reach a constant value, which increases slightly with the number of particles. This is almost identical to the result of Takasaki et al. (1993), and a slight discrepancy may be attributable to the differences of numerical schemes and the number of grid points used; e.g., 21×21 nonuniform nodal points. So we estimated the line

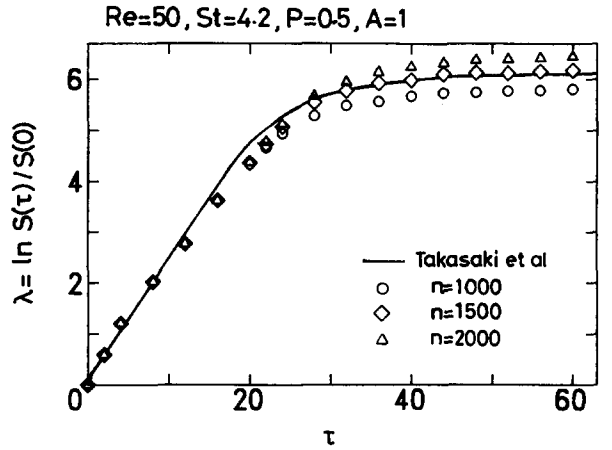

Figure 11 Time evolution of a line stretching (Re=50, St=4.2, and P=0.5)

stretching at $\tau = 20$, independent of the number of particles, as the degree of fluid mixing.

Figure 12 shows the relationship between the line stretching at $\tau = 20$ and Strouhal number for several parameters. The maximum stretching is obtained near St = 5, for $A = 1$ and 2/3. While for $A = 1/3$, the effect of Strouhal number is complicated, and the optimum Strouhal number is obtained for $4 < \mathrm{St} < 7$. Thus, we confirm that there is an optimum Strouhal number for the best mixing in each geometric aspect ratio. A comparison between $P = 0.5$ and 1.5 for $A = 1$ indicates that the amplitude of the top wall velocity has little effect on the optimum Strouhal number for the best fluid mixing. This suggests a relationship between the period of the oscillating top wall T and the turnover time of the particle motion L/v_s.

Mass transfer

Although mass transfer has been the subject of considerable attention in the steady cavity flow (see Antonini et al. 1981), there is little study on the mass transfer characteristics under time-periodic cavity flows.

When velocity and concentration fields are periodically developed within the cavity, a mean Sherwood number over a period of oscillation can be obtained by spatial integration of the instantaneous concentration gradient along the top and bottom

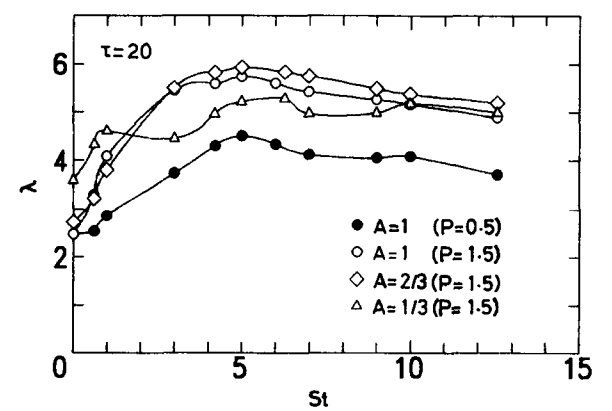

Figure 12 Line stretching at τ=20 for various flow parameters

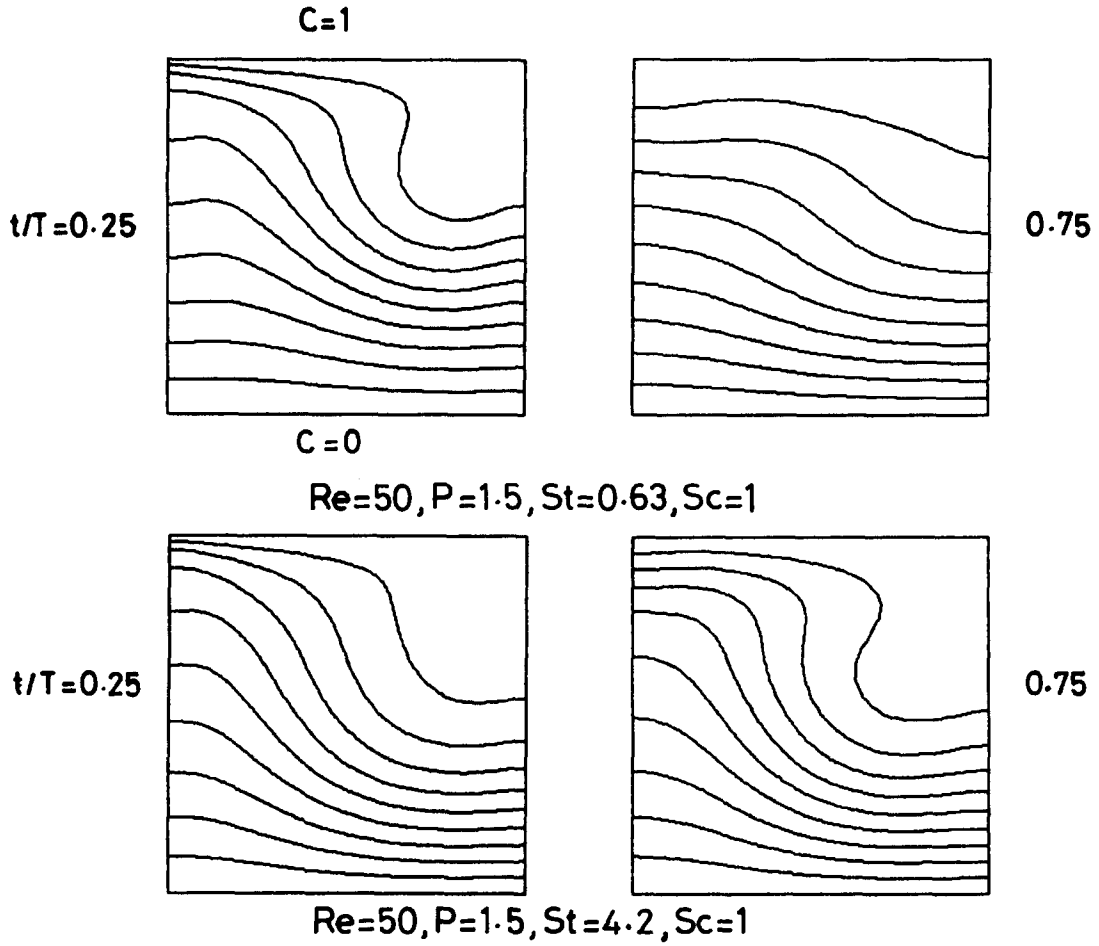

Figure 13 Concentration contours for time-periodic flows

walls as follows

$$\mathrm{Sh} = \frac{1}{2\pi A}\int_0^{2\pi}\int_0^{A}\frac{\partial c}{\partial x}\,\mathrm{d}Y\,\mathrm{d}\theta\bigg|_{x=0 \text{ or } A} \tag{7}$$

The question now is how the efficient fluid mixing mentioned above affects the transport of diffusing scalars in the flow. Figure 13 shows concentration contours for $A = 1$ at two moments during one oscillation cycle for two Strouhal numbers. One is the case of St = 0.63 for poor mixing, and the other is the case of St = 4.2 for excellent mixing. Although the concentration contours for both cases vary with time, their deformation is smaller for St = 4.2 than for St = 0.63. This is more clear in Figure 14, which shows the corresponding time variation of Sherwood numbers at the top and bottom walls. It should be noted that the time-averaged Sherwood numbers at the top and bottom walls are identical, supporting the accuracy of numerical solutions. For St = 4.2, the Sherwood number at the bottom wall varies little with time, in contrast to the result for St = 0.63.

Table 1 shows the time-averaged Sherwood number values for several Strouhal numbers. The Strouhal number is found to have little effect on the Sherwood number for $A = 1$. At St = 0.63, the Sherwood number is slightly larger than the steady flow value. However, at St = 4.2 and 12.75, they are smaller. The Strouhal number effect for $A = 2/3$ is similar, but the Sherwood numbers for $A = 1/3$ are larger than the steady flow value at Strouhal numbers considered here. This is related to a small phase difference in time variation between the top and bottom Sherwood numbers for $A = 1/3$, in contrast to the result for $A = 1$ shown in Figure 14.

The above results indicate that excellent fluid mixing does not always lead to enhancement of heat and mass transfer. This is because the critical resistance to mass transfer occurs near the bottom wall in this system, as shown in the local Sherwood numbers of Figure 14. However, the mixing near the bottom wall is poor, because the distance between trajectories of two adjacent particles near the bottom wall is very small in a given time, in contrast to the result away from the wall, as shown in Figure 15. Thus, it is suggested that when we consider the transport process from a fluid to the wall and vice versa, we must examine the local mixing where transport resistances are dominant, rather

Table 1 Time-averaged Sherwood numbers for several Strouhal numbers

	Sh		
St	A=1.0	A=2/3	A=1/3
0.0 (Steady flow)	1.740	1.640	1.159
0.63	1.754	1.653	1.239
4.2	1.711	1.622	1.185
12.57	1.711	1.624	1.163

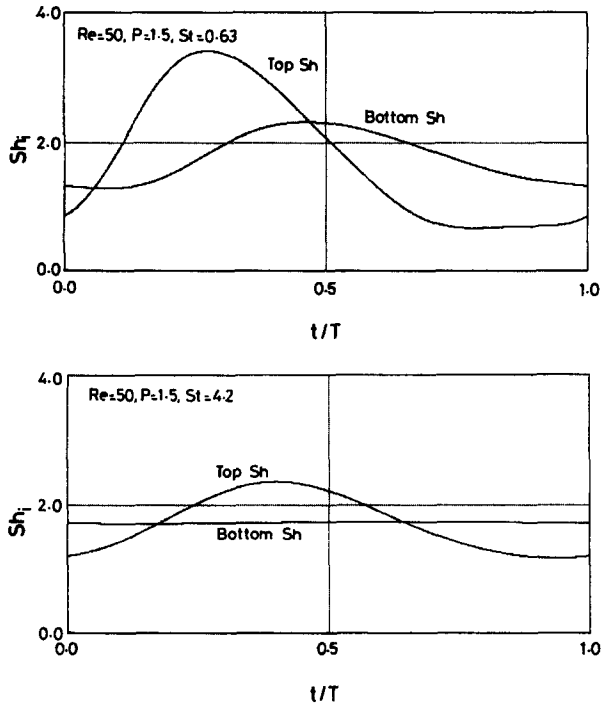

Figure 14 Time variation of Sherwood numbers at the top and bottom walls

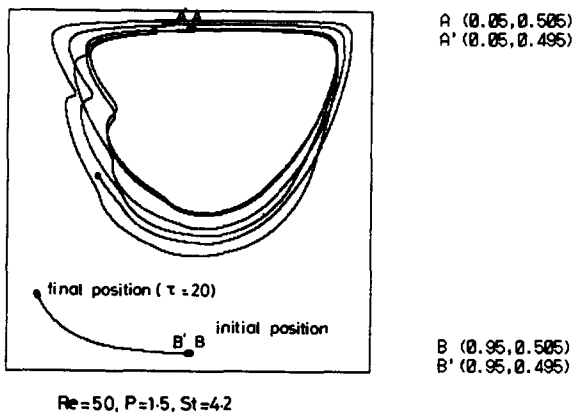

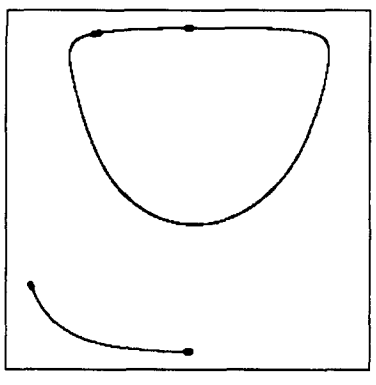

Figure 15 Trajectories of two adjacent particles for time-periodic and steady flows

than the global mixing over the system considered above. If we want mass transport enhancement in this system, we must modify the velocity boundary condition at the bottom wall. For example, the bottom wall moves in the direction opposite to the top wall, and the compositional resistance of a circulation region becomes dominant for a steady flow. However, when an unsteady component of the top wall velocity is superimposed on the steady flow, the resistance is probably reduced by excellent fluid mixing in the circulation region, as suggested from the present study. This is a subject for future work.

The information obtained here might be useful for such practical applications as etching processes of semiconductor materials and mass transfer in micromechanical devices for low-Reynolds number flows.

Conclusions

We numerically examined fluid mixing and mass transfer in cavities with time-periodic lid velocity at a low-Reynolds number. The following conclusions have been drawn.

(1) When an unsteady component of the lid velocity is superimposed on the steady flow, global fluid mixing within the cavity is greatly promoted because of the stretching and folding process of fluid particles. The degree of mixing is quantified by the stretching of a line of particles. There exists an optimum frequency of the lid velocity for the best mixing. Also, the degree of mixing increases with the amplitude of the lid velocity, but decreases for the smaller aspect ratio of the cavity.

(2) Mass transfer occurs through the fluid between the top and bottom walls of the cavity. In this system, the mean Sherwood number depends little upon the frequencies, although the instantaneous Sherwood number varies with time. This is because the local mixing near the bottom wall is poor, but the global fluid mixing is excellent. It is revealed that excellent global fluid mixing does not always lead to enhancement of heat and mass transfer.

Acknowledgments

This work was supported in part by a Grant-in-Aid for Science Research (No. 06650208) from the Ministry of Education, Science, and Culture of Japan.

References

Antonini, G., Gelus, M., Guiffant, G. and Zoulalian, A. 1981. Caracteristiques des transferts simultanés de masse et de quantité de mouvement dans des écoulements de recirculation forcée. *Int. J. Heat Mass Transfer*, **24**, 1313–1323

Aref, H. 1984. Stirring by chaotic advection. *J. Fluid Mech.*, **143**, 1–21

Biringen, S. and Danabasoglu, G. 1989. Oscillatory flow with heat transfer in a square cavity. *Phys. Fluids A*, **1**, 1796–1812

Chang, H. C. and Sen, M. 1995. Application of chaotic advection to heat transfer. In *Chaos Applied to Fluid Mixing*, H. Aref (ed.), Pergamon, Press, New York, 211–231

Ghia, U., Ghia, K. N. and Shin, C. T. 1982. High-Re solutions for incompressible flow using the Navier–Stokes equations and a multigrid method. *J. Comput. Physics*, **48**, 387–411

Ghosh, S., Chang, H. C. and Sen, M. 1992. Heat transfer enhancement due to slender recirculation and chaotic transport between counter-rotating eccentric cylinders. *J. Fluid Mech.*, **238**, 119–154

Latinopoulos, P. and Ganoulis, J. 1979. Numerical simulation of oscillating flow through idealized sclerotic arteries. *Comp. Methods Appl. Mech. Eng.*, **20**, 279–290

Mackley, M. R., Tweddle, G. M. and Wyatt, I. D. 1990. Experimental heat transfer measurements for pulsatile flow in baffled tubes. *Chem. Eng. Sci.*, **45,** 1237–1242

Nishimura, T. 1994. Heat and mass transfer enhancement by chaotic mixing in laminar flow. In *Trends in Chemical Engineering*, Vol. 2, Council of Scientific Research Integration, 199–214

Nishimura, T. 1995. Oscillatory flow and mass transfer within asymmetric and symmetric channels with sinusoidal wavy walls. Wärme und Stoffübertragung, **30,** 269–278

Nishimura, T. and Kawamura, Y. 1992. Numerical errors of the Galerkin finite-element method for natural convection of a fluid layer or a fluid-saturated porous layer. *Numer. Heat Transfer*, **22,** 241–255

Nishimura, T. and Kojima, N. 1995. Mass transfer enhancement in a symmetric sinusoidal wavy-walled channel for pulsatile flow. *Int. J. Heat Mass Transfer*, **38,** 1719–1731

Nishimura, T., Murakami, S. and Kawamura, Y. 1993. Mass transfer in a symmetric sinusoidal wavy-walled channel for oscillatory flow. *Chem. Eng. Sci.*, **48,** 1793–1800

Nishimura, T., Yoshino, T. and Kawamura, Y. 1987. Numerical flow analysis of pulsatile flow in a channel with symmetric wavy walls at moderate Reynolds numbers. *J. Chem. Eng.*, Jpn, **20,** 479–485

Ottino, J. M., Muzzio, F. J., Tjahjadi, M., Franjione, J. G., Jana, S. C. and Kusch, H. A. 1992. Chaos, symmetry, and self-similarity: Exploiting order and disorder in mixing processes. *Science* **257,** 754–760

Patera, A. T. and Mikic, B. B. 1986. Exploiting hydrodynamic instabilities, resonant heat transfer enhancement. *Int. J. Heat Mass Transfer*, **29,** 1127–1138

Saatdjian, E., Dardour, B. and Mota, J. P. B. 1995. Heat transfer enhancement by chaotic advection and recirculation in the annular region between confocal ellipses. In *Numerical Methods in Laminar and Turbulent Flows '95*, C. Taylor and P. Durbetaki (eds.), Pineridge Press, 229–239

Takasaki, S., Ogawara, K. and Iida, S. 1993. A study on chaotic mixing in two-dimensional cavity flows. *Nagare* **12,** 20–30